A Letters Journal Exploring the Frontiers of Physics

September 2021

EPL, **135** (2021) 58001
doi: 10.1209/0295-5075/135/58001

www.epljournal.org

Balancing efficiency and homogeneity of biomaterial transport in networks

Susanne Liese[1(a)], L. Mahadevan[2,3] and Andreas Carlson[1(b)]

[1] *Department of Mathematics, Mechanics Division, University of Oslo - N-0851, Oslo, Norway*
[2] *Department of Physics, Harvard University - Cambridge, MA 02138, USA*
[3] *Department of Organismic and Evolutionary Biology, Harvard University - Cambridge, MA 02138, USA*

received 8 March 2021; accepted in final form 16 August 2021
published online 2 November 2021

Abstract – Transport of biomaterial in tubular networks is ubiquitous in nature, where examples include the endoplasmic reticulum, leaf venation or vessel networks in vertebrates. Flow feedback by adjustment of the local tube radius in response to a fluid flow is a pivotal mechanism to optimize the transport properties of a network. To describe liquid transport in tubular networks we develop a minimal mathematical model, which includes the interplay of the viscous flow feedback and the tubes elastic bending energy while conserving the network material. Flow feedback in *pitted*, *branched* and *loopy* networks is shown to lower their resistance, as compared to a feedback-free system, by local adaptations without the need for additional network material. Flow feedback in particular reduces the resistance in *pitted* and *branched* networks, directly linked with a reduction in the effective number of neighboring tubes. In loopy networks we find a direction-dependent flow resistance, with a prevailing transport direction set by the network geometry.

Introduction. – Transport of biomaterials in tubular networks is widespread in nature, where examples include the subcellular endoplasmic reticulum, the venation network in leaves and the vascular network of the human body [1–3]. Biological networks are typically highly dynamic and are found on various length and time scales: Three-way junctions in the endoplasmic reticulum show movements on the scale of nm over several seconds [1], vessels in brain vascular networks ($\sim$ μm) form over a time span of hours and slime mold and fungi grow stable networks ($\sim$ cm) over hours or days [4–6]. These networks span large distances and provide an efficient way for transport and signal propagation as part of biological communication pathways [2,7,8]. It seems natural to ask, which structural features optimize the transport properties? Theoretical studies have investigated the development of an optimal network structure under constant cost [9–11], where the cost was considered to be proportional to $\sim C^\gamma$, with C the conductance and $\gamma > 0$ an exponent that reflects the biophysical nature of the network. In these studies an optimal network is considered to be a network that minimizes the total power dissipation, *i.e.*, a global property. Under this condition a phase transition of the optimal network structure is observed, from branched/tree-like to loopy networks, at $\gamma = 1$. Two alternative measures that both can be considered as a criterion for optimal transport are the global viscous flow resistance and the homogeneity of the flow distribution. A low viscous resistance is desirable to speed up the transport of liquid biomaterials across large distances, whereas a homogeneous flow distribution enables an even distribution of biomaterial in the network. Both criteria, flow efficiency and flow homogeneity, need to be balanced for the network to fulfill multiple functionalities.

Biological networks adopt different structures depending on their functionality, where we can distinguish branched/tree-like networks and loopy networks [10,12]. A general characteristic of a branched network is a high transport efficiency while retaining a small surface area. At the same time, a branched network is vulnerable to the damage of individual network edges, which hinders down-stream transport [13]. A loopy network, on the other hand, contains multiple pathways between any two network nodes, which provides resilience to edge damage [10, 14]. Theoretical work has also found that flow fluctuations can stabilize loopy networks [10,15]. Biological networks adapt their structure in different ways: The network can

[(a)] Current address: Max Planck Institute for the Physics of Complex Systems - D-01187 Dresden, Germany.
[(b)] E-mail: acarlson@math.uio.no (corresponding author)

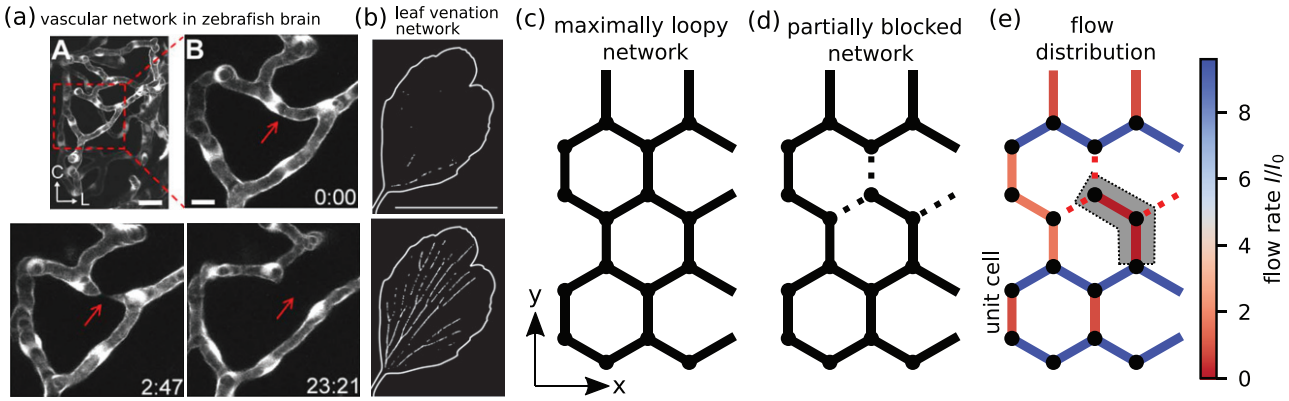

Fig. 1: (a) In the vascular network in zebrafish brains, low transport of biomaterial makes tubes shrink and vanish over time. Scale bar, 25 μm in A and 10 μm in B. The time is indicated at the lower right corner of the panels (h: min). Figure adapted from ref. [18]. (b) In leaf venation networks, embolism forms during leaf drying. Scale bar: 5 mm. Time: 2h 5min (top), 4h 10min (bottom). Figure adapted from ref. [19]. (c) The membrane tube network is modeled as a hexagonal grid. The network section depicted here consists of two unit cells in x-direction and y-direction. (d) Three of the 24 tubes are randomly selected and blocked (dashed lines), *i.e.*, the flow rate is $I = 0$. (e) A pressure difference of $\Delta p/\Delta p_0 = 10$ is applied horizontally. Periodic boundary conditions are applied in both directions in space. The resulting flow rate in each tube is shown on the color bar. Blue lines correspond to a high flow rate, where the flow feedback promotes an increase of the tube radius, whereas red lines show a low flow rate, which leads to a shrinking of the tube radius, due to the overall area conservation. In addition to the blocked tubes, two tubes are part of a "dead-end" (gray shaded box), *i.e.*, they cannot transport flow due to the lack of open connecting tubes.

expand and create new connections [16,17], or existing network edges can be blocked or retracted [18,19]. A series of theoretical studies have investigated the transport properties of bio-inspired hexagonal networks [9–11,20–23]. It was shown among other things that the removal and addition of network edges, as well as adjusting edge conductance, optimize the transport properties to fulfill different or multiple functionalities [20–22], where local adaptations are able to optimize the global transport properties [23,24].

The growth of a network and the formation of new connections is bio-mechanically challenging and typically energetically costly. Feedback loops, in which the transport-efficient pathways are further strengthened, can take advantage of the existing network to optimise the network properties [25–27]. Prominent examples that exhibit feedback in networks are slimemolds, which grow in such a way that they generate optimal connections with nutrition sources [6,28]. A similar principle is found in flow-induced feedback in tubular networks both in animals and in plants [29], where a high flow rate leads to an increase of the tube radius, while a low flow rate causes tubes to vanish over time [17,18,30] (fig. 1(a)).

In the present study, we investigate how flow feedback modulates the transport properties of an elastic network, where the total area, *i.e.*, the amount of network material is conserved. We consider a tubular network, where flow along the tubes follows a Hagen-Poiseuille flow and the total mass flux is conserved. We impose that the radii and lengths of the network tubes are subjected to elastic energy minimization and area conservation. In addition, the flow through the tubes induces a feedback that acts to increase the tube radius. While many biological networks are known to have a reticulated structure that is characterised by a large number of loops [10], the network structure can be altered by retraction of network tubes, as was observed in the vascular network in zebrafish brains [18] (fig. 1(a)), or embolism during leaf desiccation [19] (fig. 1(b)). The structure of biological networks can be altered by permanent or transient blockage of network tubes, seen at different length scales, *e.g.*, clogging of blood vessels causing thrombosis and atherosclerosis [31,32] or membrane nanotubes that can be constricted by various proteins [33]. To investigate the influence of networks with different degrees of connectivity, we block some of the tubes, *i.e.*, these tubes cannot participate in the flow transport, to create loopy, branched and pitted networks. For each network we determine the global flow resistance and the distribution of the flow current, which allows us to connect different measures for an optimal transport within the network structure.

Mathematical model and computational methods. – We consider a minimal representation of a dynamic, biological network that incorporates the key characteristics of tubular membrane networks, where neighboring nanotubes are connected via y-junctions, similar to natural and synthetic membrane networks [1,34]. The network is modeled as a two-dimensional, hexagonal grid (fig. 1), with n_x, n_y unit cells in x- and y-direction, where each unit cell contains four nodes and six tubes (fig. 1(c)–(e)). The length of the simulation box in the x- and y-direction, L_x, L_y, is fixed, with $L_x = n_x\sqrt{3}L_0$,

$L_y = 3L_0$ and L_0 the initial tube length. For a given n_x we chose n_y such that the simulation box approximates as closely as possible to a square shape. The size of the simulation box is then defined as $L_{\mathrm{box}} = \sqrt{L_x L_y}$. In the initial configuration, neighboring tubes form an angle of 120°, which is known to optimize the transport efficiency in static networks [35]. We assume that the total surface area of the tubes is conserved, which in a membrane network corresponds to a conservation of lipid mass. We apply a constant pressure difference per unit length Δp across the network, which causes a flow rate $I_{i,j}$ along the network edges, where the subscript i, j, refers to the node indices in the x-y plane. Δp appears in the description of the local flow rate in the network instead of explicitly as a boundary condition. For large networks Δp has the equivalent effect of a pressure difference $\Delta P = \Delta p L_{\mathrm{box}}$ that is applied at the periodic boundaries of the simulation box. By assuming a viscous flow in the tubes described by a Hagen-Poiseuille flow [23], we can then write

$$I_{i,j} = \frac{\pi R_{i,j}^4}{8\mu}\left(\frac{P_i - P_j}{L_{i,j}} + \Delta p \mathbf{e}_p \mathbf{e}_{i,j}\right), \tag{1}$$

with $R_{i,j}$ and $L_{i,j}$ the tube radius and length, μ the dynamic viscosity, P_i the pressure at node i and $\mathbf{e}_p$, $\mathbf{e}_{i,j}$ unity vectors in the direction of the external pressure difference and the edge i, j, respectively. Thus, pressure acts similarly to a global strain in a mechanical network.

In addition, we impose mass conservation that implies

$$\sum_j I_{i,j} = 0. \tag{2}$$

In the feedback-free case, the ratio between the tube length and radius is set by the minimization of the bending energy

$$E_{\mathrm{bend}} = \frac{1}{2}\sum_{i,j} \pi\kappa \frac{L_{i,j}}{R_{i,j}}, \tag{3}$$

with the bending rigidity κ [36]. By considering a box with fixed size and periodic boundary conditions, all tubes adopt the same radius R_0 and length L_0. The area is constrained by a harmonic potential with

$$E_{\mathrm{const}} = \frac{20\pi\kappa}{R_0^4 n_x n_y}\left(6 n_x n_y R_0 L_0 - \frac{1}{2}\sum_{i,j} R_{i,j} L_{i,j}\right)^2. \tag{4}$$

The time evolution of the tube radii can now be written as

$$\frac{\mathrm{d}R_{i,j}}{\mathrm{d}t} = -\gamma \frac{\mathrm{d}(E_{\mathrm{bend}} + E_{\mathrm{const}})}{\mathrm{d}R_{i,j}} + \epsilon \frac{I_{i,j}}{I_0 + I_{i,j}}, \tag{5}$$

where the second term on the right-hand side accounts for the flow feedback that can increase the local tube radius. We model the feedback as a Hill-like response, where the feedback rate ϵ controls the strength of the feedback and I_0 denotes the fluid flow rate through a single tube of radius R_0 if a reference pressure difference Δp_0 is applied between the ends of the tube.

The time evolution of the positions of the network nodes $\mathbf{r}_i = [x_i, y_i]^{\mathrm{T}}$ is given by

$$\frac{\mathrm{d}\mathbf{r}_i}{\mathrm{d}t} = -\gamma \nabla_i (E_{\mathrm{bend}} + E_{\mathrm{const}}), \tag{6}$$

with γ the friction factor that sets the time scale for conformation relaxation in a feedback-free network. The shift of the node position leads to a change in the tube lengths, which are, however, small compared to the initial tube length (see the Supplementary Material `Supplementarymaterial.pdf` (SM)).

To non-dimensionalise the model we scale all lengths by R_0 and time by $t_0 := R_0^2/(\gamma\pi\kappa)$, which introduced into eq. (5) and eq. (6) gives the non-dimensional number for the scaled feedback rate as $\bar{\epsilon} := \epsilon R_0/(\gamma\pi\kappa)$. We integrate the non-dimensional eqs. (5), (6) numerically with a time step of $\Delta t = 10^{-4} t_0$ over 30000 steps. Periodic boundary conditions are applied in both directions in space. To generate partially blocked networks up to 35% of the tubes are clogged, *i.e.*, the fluid flow rate $I_{i,j}$ through these tubes is set to zero. The area of the clogged tubes is included in the total area of the system and is therefore subject to the area constraint. Since flow feedback causes tubes with high flow rates to become larger, the area constraint can cause clogged tubes to decrease in size. The clogged tubes are selected with the constraint that each node must be connected to any other node along at least one pathway. In fig. 1(e) a network section is shown, where three of the 24 tubes are blocked. In addition, two tubes are part of "dead-end", which refers to tubes that are not blocked, but nevertheless have a zero flow rate due to the lack of open neighboring tubes. To quantify the connectivity of the network, we defined the effective number of neighbors N_{eff}, which is the number of connecting tubes for each node that are neither blocked nor part of a dead-end and averaged over the entire network. If none of the tubes are blocked $N_{\mathrm{eff}} = 3$ and each node can be reached on multiple paths. We define a network with $N_{\mathrm{eff}} \geq 2.5$ as a loopy network. In a branched network, where all nodes are connected along a single pathway, each node has two neighboring tubes. Hence, networks with $1.5 \leq N_{\mathrm{eff}} < 2.5$ are defined as branched networks. For $N_{\mathrm{eff}} < 1.5$ there must be nodes in the network that are only connected to blocked or dead-end tubes. Networks with $N_{\mathrm{eff}} < 1.5$ are classified as pitted networks. To investigate the direction-dependent flow resistance in maximally loopy networks ($N_{\mathrm{eff}} = 3$, fig. 2) we use networks with $n_x = 3$ unit cells in the x- and $n_y = 2$ unit cells in the y-direction. The simulation of partially blocked networks are performed with $n_x = 6$, $n_y = 4$. The transport properties in each network are determined by two non-dimensional parameters, the feedback strength $\bar{\epsilon}$ and the scaled pressure difference $\Delta p/\Delta p_0$. In other words, after normalization of time and length, the flow is set by two quantities that are governed by the feedback mechanism. If not indicated otherwise the feedback strength and the pressure difference are set to $\bar{\epsilon} = 10$ and $\Delta p/\Delta p_0 = 10$. Smaller values for $\bar{\epsilon}$ lead to

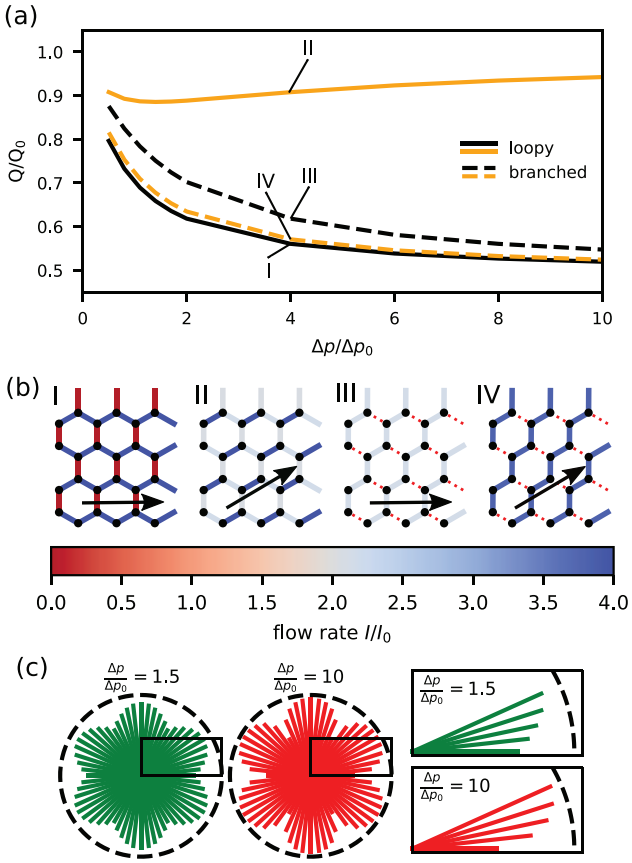

Fig. 2: (a) Flow resistance Q scaled by the resistance of a feedback-free network Q_0 as a function of the pressure difference $\Delta p/\Delta p_0$. The pressure difference is either aligned with the x-axis (black lines) or forms an angle of 30° with the x-axis (orange lines). The networks constitute either loopy (solid lines) or branched (dashed lines) networks as depicted in panel (b). (b) The flow rate in each tube is shown on the color bar for $\Delta p/\Delta p_0 = 4.0$. The direction of the pressure is indicated by the arrow. Two loopy (I, III) and two branched (II, IV) networks are shown. (c) The length of each line shows the flow resistance Q scaled by the resistance in a feedback-free network Q_0, while the orientation of each line is aligned with the direction of the pressure in a loopy network. The flow resistance in a feedback-free network is shown as a dashed, black line. The inset on the right-hand side shows the flow resistance for five different tilt angles between 0° and 30°.

a less pronounced resistance reduction, but give the same qualitative pressure dependence (see the SM).

Results and discussion. – To study the effect a flow-induced feedback has on transport properties of the tubular network, we first consider maximally loopy networks ($N_{\text{eff}} = 3$), where all tubes are open and hence able to transport liquid. We vary the direction of the pressure difference, which allows us to study the direction dependent flow resistance. Afterwards, we perform simulations on partially blocked networks to answer the question: how does the flow feedback affects branched networks?

Directional dependent flow resistance. We start by evaluating the global flow resistance Q, as the direction of the pressure difference is varied. To determine the resistance, we first define the dissipation rate in each tube $W_{i,j}$:

$$W_{i,j} = \frac{8\mu L_{i,j}}{\pi R_{i,j}^4} I_{i,j}^2, \tag{7}$$

with $8\mu L_{i,j}/(\pi R_{i,j}^4)$ the resistance of an individual tube. The global resistance is defined based on the dissipation rates $W_{i,j}$ and the pressure difference ΔP as

$$Q = \frac{(\Delta P)^2}{\frac{1}{2}\sum_{i,j} W_{i,j}}. \tag{8}$$

We compare two types of networks, loopy networks (solid lines in fig. 2(a) and configurations I, II in fig. 2(b)) and branched networks (dashed lines in fig. 2(a) and configurations III, IV in fig. 2(b)), where individual tubes are clogged, such that the flow transport across the network occurs along a single pathway. The pressure difference is applied either parallel to the x-axis (black lines in fig. 2(a), I, III in fig. 2(b)) or with an angle of 30° (orange lines in fig. 2(a), II, IV in fig. 2(b)). Due to the symmetry of the hexagonal network, a rotation of more than 30° leads to equivalent point symmetric configurations. The tilt angles of 0° and 30° are thus the two extreme cases with respect to the pressure direction.

In a feedback-free scenario, *i.e.*, when the flow does not modulate the tube radius, the network resistance is given by $Q_0 = 8\sqrt{3}\mu L_0/(\pi R_0^4)$ and the resistance is independent of the direction and magnitude of the pressure difference. Figure 2(a) shows Q (eq. (8)) as a function of $\Delta p/\Delta p_0$. We now find in fig. 2(a) that the flow feedback causes a pressure-dependent resistance, where Q depends on both the magnitude of $\Delta p/\Delta p_0$ and the orientation of the pressure difference relative to the network. Loopy networks show a distinctively different behavior depending on the pressure direction. If the pressure is applied horizontally (black, solid line in fig. 2(a)) Q exhibits a steep decrease for small Δp and continues to decrease over the entire range of Δp. In contrast, if the direction of the pressure drop is tilted by 30° (orange, solid line in fig. 2(a)), Q exhibits a minimum around $\Delta p/\Delta p_0 = 1.5$ before it approaches the resistance of a feedback-free network for large pressure differences. In contrast, branched networks exhibit a monotonic decrease of Q for both pressure directions.

To understand the directional dependent pressure response in loopy networks, we examine the flow distribution shown in fig. 2(b) (I, III). In the first case (I) one third of the tubes lie perpendicular to the pressure difference and hence exhibit no flow. Only the tubes that are already partially aligned with the pressure gradient have a non-zero flow rate and therefore experience a flow-driven increase of their radii, which in turn causes an effectively reduced resistance. In the second case (III) all tubes show non-zero flow rates. If the flow rate is much larger than

I_0, all tubes experience a similarly strong feedback, but the radius expansion is limited by the area conservation. Hence, the conformation of the network, in particular the radii of the tubes remain close to the feedback-free case. In the branched networks (II, IV), on the other hand, flow transport follows one single pathway independent of the pressure direction, where the blocked tubes serve as a material reservoir that allows the adjacent tubes to increase their radii and subsequently lower the network resistance.

To further analyze the directional dependent resistance in loopy networks, we show Q (eq. (8)) in fig. 2(c) for different pressure directions for $\Delta p = 1.5\Delta p_0$ (green line) and $\Delta p = 10\Delta p_0$ (red line). The length of each line indicates the resistance relative to the resistance of a feedback-free network and the angle relative to the x-axis shows the direction of the pressure difference. The direction dependence of Q mimics the six-fold geometry of the hexagonal network. Q is lowest, if parts of the tubes lie perpendicular to the pressure difference, while Q increases to values close to the feedback-free scenario, if the network edges are aligned with the pressure difference direction.

Partially blocked networks. We now turn to partially blocked networks, to investigate how flow feedback influences networks with different structure, focussing in particular on branched and loopy networks. The pressure direction forms an angle of either 0° or 30° with respect to the x-axis. Figure 3(a) presents examples of a pitted, a branched and a loopy network. The blocked tubes are shown as dashed lines. Tubes with a high flow rate of more than $I_0/3$ are shown in blue, while tubes with a low flow rate of less than $I_0/3$ are shown in red.

We have so far discussed the resistance as a measure for an efficient transport through the network. However, Q does not contain information about how uniformly the flow is distributed throughout the network. To quantify the flow distribution, we evaluate the current

$$M_i = \sqrt{\frac{1}{2}\sum_j I_{i,j}^2} \tag{9}$$

through each node as the quadratic mean of the flow rates of the adjacent tubes. To describe the flow distribution by means of a single quantity, we define the inhomogeneity $\mathcal{M}$ as

$$\mathcal{M} = \frac{\Delta M}{\langle M \rangle}, \tag{10}$$

where the mean $\langle M \rangle$ and the standard deviation ΔM are taken over the entire network. Low values of $\mathcal{M}$ indicate a homogenous flow distribution.

First, we evaluate how the transport properties of a feedback-free network depend on the effective number of neighbors N_{eff}. In fig. 3(b) and (c) the resistance scaled by the resistance of a loopy network with $N_{\text{eff}} = 3$ and the inhomogeneity $\mathcal{M}$ are shown as a function of the effective number of neighbors. The subscript 0 indicates that the feedback rate $\bar{\epsilon}$ is set to zero. Figures 3(b) and (c) show that pitted and branched networks exhibit low resistance

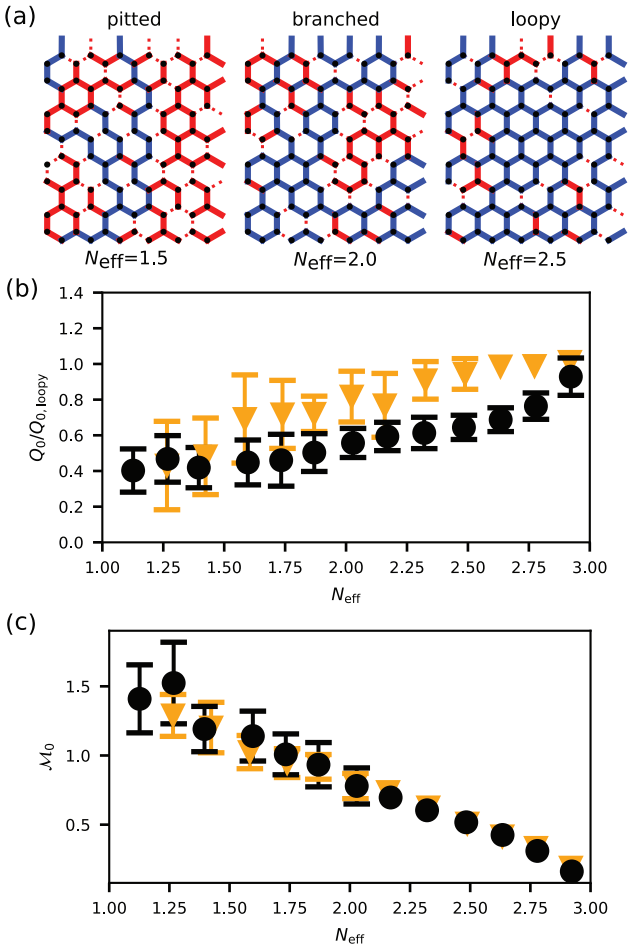

Fig. 3: (a) A schematic illustration of pitted, branched and loopy networks with randomly blocked tubes. Blocked tubes are shown as dashed lines. Tubes with a flow rate of more/less than $I_0/3$ are shown in blue/red. (b) The flow resistance Q_0 in a feedback-free network scaled by the flow resistance $Q_{0,\text{loopy}}$ in a loopy network with $N_{\text{eff}} = 3$ as a function of the effective number of next neighbors N_{eff}. The pressure difference is applied with a tilt angle of 0° (circular markers) or 30° (triangular markers) relative to the x-axis. We bin N_{eff} with a bin width of 0.15 and average $Q_0/Q_{0,\text{loopy}}$ of at least ten simulation runs. The standard deviation is indicated by the error bar, if it is larger than the symbol size. (c) The inhomogeneity $\mathcal{M}$ is shown as a function of the effective number of next neighbors N_{eff}. The marker symbols are chosen in analogy to panel (b).

as compared to loopy networks, which can be attributed to the smaller number of network links. In contrast, loopy networks, where a larger fraction of the network edges participate in flow transport, maintain a more homogeneous flow distribution.

We now turn to describe the effect of flow feedback. In fig. 4(a) we show how the flow resistance Q is coupled to the effective number of neighbors N_{eff}. Q is scaled by Q_0, the resistance in a feedback-free network, where the same tubes are blocked. Figure 3(a) shows that the flow feedback induces a reduction of the flow resistance for all systems investigated. The relative flow resistance

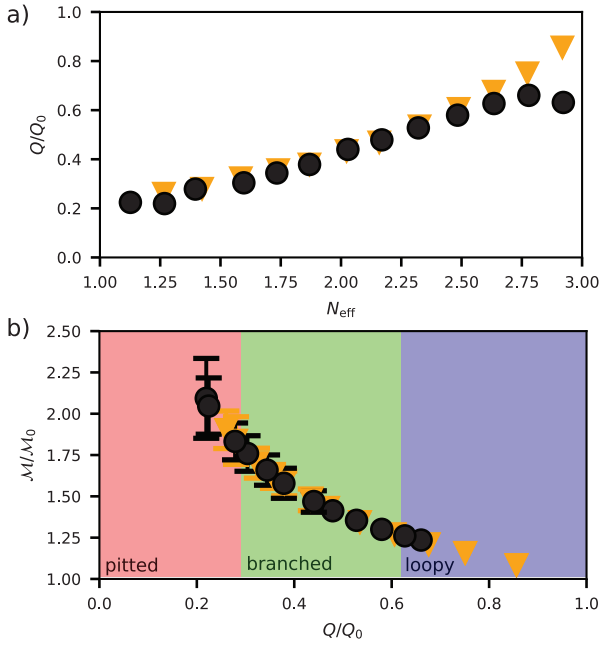

Fig. 4: (a) The flow resistance Q as a function of the effective number of next neighbors N_{eff}. Q is scaled by the resistance in a feedback-free network with the same blocked tubes. The marker symbols are chosen in analogy to fig. 3(b). (b) Homogeneity $\mathcal{M}$ as a function of the scaled flow resistance Q/Q_0. The marker symbols are chosen in analogy to fig. 3(b). We have classified the networks as: pitted ($N_{\mathrm{eff}} < 1.5$), branched ($1.5 \leq N_{\mathrm{eff}} < 2.5$) or loopy ($N_{\mathrm{eff}} \geq 2.5$).

Q/Q_0 is smallest for networks with low connectivity, *i.e.*, low N_{eff}. We attribute the resistance reduction to the large reservoir of tube material or equivalently tube surface in the blocked or dead-end tubes, which can be exploited by the high flow rate tubes to increase their radius. A direction-dependent resistance is only found in loopy networks with $N_{\mathrm{eff}} \gtrsim 2.75$. We attribute this maximum to the network structure. If the pressure in loopy networks is parallel to the x-axis, the transport is determined solely by the tubes parallel to the x-axis. If a small number of these tubes are blocked, the flow must be diverted via perpendicularly running tubes. The feedback mechanism cannot compensate for the resulting loss of efficiency, which leads to an increase in resistance. In branched systems, or when the pressure is tilted by 30°, there is an alternative nearly parallel transport path. If a path is blocked, the alternative flow path is further enhanced by the feedback leading to a decrease in relative resistance. Figure 4(b) shows $\mathcal{M}/\mathcal{M}_0$ as a function of the scaled resistance Q/Q_0. The regions that correspond to pitted, branched and loopy networks are indicated in different colors. Independently of the pressure direction, we see that the weak resistance reduction (large Q/Q_0) that we find in loopy networks allows to maintain a homogeneous flow distribution (low $\mathcal{M}/\mathcal{M}_0$). In contrast, pitted networks experience a significant flow reduction (low Q/Q_0), which at the same time leads to an increased inhomogeneity of the flow distribution (large $\mathcal{M}/\mathcal{M}_0$). Branched networks show an intermediate resistance reduction as well as an increase of flow inhomogeneity.

Conclusion. – We investigate how flow feedback in an elastic tubular network effects the transport properties of viscous fluids and how flow efficiency and flow distribution are related to the network structure. The results shown in fig. 2 reveal two major aspects of flow transport in maximally loopy networks. 1) Flow feedback lowers the resistance as compared to a feedback-free network, without the need for additional network material. The resistance reduction is achieved solely by redistributing network material, *i.e.*, adjusting the tube radii and the position of the nodes. Thus, flow feedback provides an efficient way to change global network properties by a local adaptation rule, similar to the optimization of flow dissipation that was found in leaf-like venation networks [10,23]. 2) We find that the resistance reduction in loopy networks is direction dependent, which allows the network to combine major aspects of loopy and tree-like networks. Similar to tree-like networks, we find a prevailing transport direction that is set by the network structure. At the same time, each node keeps a large number of connections to its neighbors, which is known to give a network mechanical stability and resilience to edge damage [21].

The results in fig. 3 for partially blocked networks highlight that different network functionalities require antagonistic network properties. A strong flow feedback isdesirable, if the optimal network requires a low flow resistance, whereas weak or no flow feedback is beneficial to achieve a uniform flow distribution. A biological network fulfilling multiple functionalities needs to balance different transport properties, which can be achieved by adjusting the network structure. We show that loopy networks are less affected by flow feedback, both in terms of flow resistance and flow distribution, than pitted and branched networks. Based on the results presented here, we hypothesize that different network functionalities can be optimized simultaneously in patched or hierarchical network structures that combine loopy and branched networks portions, a trait recurring in many reticulated biological networks [1–3,37,38].

REFERENCES

[1] Nixon-Abell J., Obara C. J., Weigel A. V., Li D. *et al.*, *Science*, **354** (2016) aaf3928.
[2] Roth-Nebelsick A., Uhl D., Mosbrugger V. and Kerp H., *Ann. Bot.*, **87** (2001) 553.
[3] Red-Horse K. and Siekmann A. F., *Bioessays*, **41** (2019) 3.
[4] Nakagaki T., Kobayashi R., Nishiura Y. and Ueda T., *Proc. R. Soc. B: Biol. Sci.*, **271** (2004) 2305.
[5] Bebber D. P., Hynes J., Darrah P. R., Boddy L. *et al.*, *Proc. R. Soc. B: Biol. Sci.*, **274** (2007) 2307.
[6] Tero A., Takagi S., Saigusa T., Ito K. *et al.*, *Science*, **327** (2010) 439.

[7] Carmeliet P. and Tessier-Lavigne M., *Nature*, **436** (2005) 193.
[8] Davidson A. J. and Wood W., *Trends Cell Biol.*, **26** (2016) 569.
[9] Banavar J., Colaiori F., Flammini A., Maritan A. *et al.*, *Phys. Rev. Lett.*, **84** (2000) 4745.
[10] Katifori E., Szollosi G. J. and Magnasco M. O., *Phys. Rev. Lett.*, **104** (2010) 4.
[11] Kirkegaard J. B. and Sneppen K., *Phys. Rev. Lett.*, **124** (2020) 20.
[12] Ronellenfitsch H. and Katifori E., *Phys. Rev. Lett.*, **123** (2019) 24.
[13] Katifori E., *C. R. Phys.*, **19** (2018) 244.
[14] Kaiser F., Ronellenfitsch H. and Witthaut D., *Nat. Commun.*, **11** (2020) 1.
[15] Corson F., *Phys. Rev. Lett.*, **104** (2010) 4.
[16] Hall C. N., Reynell C., Gesslein B., Hamilton N. B. *et al.*, *Nature*, **508** (2014) 55.
[17] Marcos D. and Berleth T., *Front. Plant Sci.*, **5** (2014) 235.
[18] Chen Q., Jiang L., Li C., Hu D. *et al.*, *PLoS Biol.*, **10** (2012) 8.
[19] Brodribb T. J., Bienaime D. and Marmottant P., *Proc. Natl. Acad. Sci. U.S.A.*, **113** (2016) 4865.
[20] Meigel F. J. and Alim K., *J. R. Soc. Interface*, **15** (2018) 142.
[21] Rocks J. W., Ronellenfitsch H., Liu A. J., Nagel S. R. and Katifori E., *Proc. Natl. Acad. Sci. U.S.A.*, **116** (2019) 2506.
[22] Ocko S. A. and Mahadevan L., *Phys. Rev. Lett.*, **114** (2015) 13.
[23] Hu D. and Cai D., *Phys. Rev. Lett.*, **111** (2013) 13.
[24] Rocks J. W., Liu A. J. and Katifori E., *Phys. Rev. Lett.*, **126** (2021) 2.
[25] Haskovec J., Jonsson H., Kreusser L. M. and Markowich P., *Proc. R. Soc. A: Math. Phys. Eng. Sci.*, **475** (2019) 2231.
[26] Paul T. J. and Kollmannsberger P., *PLoS Comput. Biol.*, **16** (2020) 11.
[27] Biedron M. and Banasiak A., *Plant Cell Rep.*, **37** (2018) 1215.
[28] Alim K., Andrew N., Pringle A. and Brenner M. P., *Proc. Natl. Acad. Sci. U.S.A.*, **114** (2017) 5136.
[29] Meigel F. J., Cha P., Brenner M. P. and Alim K., *Phys. Rev. Lett.*, **123** (2019) 228103.
[30] Dahl-Jensen S. B., Yennek S., Flasse L., Larsen H. L., Sever D., Karremore G., Novak I., Sneppen K. and Grapin-Botton A., *PLoS Biol.*, **16** (2018) 7.
[31] Ross R., *Nature*, **362** (1993) 801.
[32] Furie B. and Furie B. C., *New Engl. J. Med.*, **359** (2008) 938.
[33] Bassereau P., Jin R., Baumgart T., Deserno M. *et al.*, *J. Phys. D: Appl. Phys.*, **51** (2018) 34.
[34] Bilal T. and Gozen I., *Biomater. Sci.*, **5** (2017) 1256.
[35] Durand M. and Weaire D., *Phys. Rev. E*, **70** (2004) 2.
[36] Helfrich W., *Z. Naturforsch. C*, **28** (1973) 693.
[37] Sack L., Scoffoni C., McKown A. D., Frole K. *et al.*, *Nat. Commun.*, **3** (2012) 837.
[38] Karschau J., Scholich A., Wise J., Morales-Navarrete H., Kalaidzidis Y., Zerial M. and Friedrich B. M., *PLoS Comput. Biol.*, **16** (2020) 6.